Mutations in the NB-ARC Domain of I-2 That Impair ATP Hydrolysis Cause Autoactivation[1][OA]

Wladimir I.L. Tameling[2,3], Jack H. Vossen[2,4], Mario Albrecht, Thomas Lengauer, Jan A. Berden, Michel A. Haring, Ben J.C. Cornelissen, and Frank L.W. Takken*

Plant Pathology (W.I.L.T., J.H.V., B.J.C.C., F.L.W.T.), Biomolecular Mass Spectrometry (J.A.B.), and Plant Physiology (M.A.H.), Swammerdam Institute for Life Sciences, University of Amsterdam, 1090 GB Amsterdam, The Netherlands; and Max Planck Institute for Informatics, 66123 Saarbruecken, Germany (M.A., T.L.)

Resistance (R) proteins in plants confer specificity to the innate immune system. Most R proteins have a centrally located NB-ARC (nucleotide-binding adaptor shared by APAF-1, R proteins, and CED-4) domain. For two tomato (*Lycopersicon esculentum*) R proteins, I-2 and Mi-1, we have previously shown that this domain acts as an ATPase module that can hydrolyze ATP in vitro. To investigate the role of nucleotide binding and hydrolysis for the function of I-2 in planta, specific mutations were introduced in conserved motifs of the NB-ARC domain. Two mutations resulted in autoactivating proteins that induce a pathogen-independent hypersensitive response upon expression in planta. These mutant forms of I-2 were found to be impaired in ATP hydrolysis, but not in ATP binding, suggesting that the ATP- rather than the ADP-bound state of I-2 is the active form that triggers defense signaling. In addition, upon ADP binding, the protein displayed an increased affinity for ADP suggestive of a change of conformation. Based on these data, we propose that the NB-ARC domain of I-2, and likely of related R proteins, functions as a molecular switch whose state (on/off) depends on the nucleotide bound (ATP/ADP).

To survive, multicellular organisms had to evolve ways to defend themselves against pathogens. This has led to the evolution of passive and active immune responses of which the latter can be divided in adaptive and innate immunity. Whereas the adaptive system is only found in vertebrates, innate immunity seems to be more ancient because it is widely spread across kingdoms (ranging from humans, flies, and nematodes to plants). For induction of the innate immune response, the host first has to perceive pathogen attack. Recognition of pathogen-derived elicitors is mediated by specialized receptors; in animals, these are represented by pattern recognition receptors (Inohara and Nunez, 2003) and in plants by resistance (R) proteins (Dangl and Jones, 2001). Following recognition, there is an activation of downstream-signaling pathways leading to disease resistance and often a hypersensitive response (HR) that is manifested as cell death (Dangl and Jones, 2001).

Most *R* genes encode proteins with a predicted trimodular structure (Inohara and Nunez, 2003; Martin et al., 2003). At their carboxy terminus, these trimodular proteins carry a Leu-rich repeat (LRR) domain believed to be the initial recognition domain for the following reasons: (1) This domain is highly variable and under divergent selection (Meyers et al., 2002); and (2) functional analysis has indicated that specific recognition of pathogens resides in this domain (Ellis et al., 2000). The trimodular R proteins have either an amino-terminal domain that contains coiled-coil (CC) motifs or a domain that shares homology to the Toll/interleukin-1 receptor (Pan et al., 2000b). Since the amino-terminal domain appears to determine the requirement for certain signaling components, such as EDS1 or NDR1, it is generally believed that this part is important for downstream signaling (Feys and Parker, 2000). At the center of the R protein, we find the NB-ARC (nucleotide-binding adaptor shared by APAF-1, R proteins, and CED-4) domain (van der Biezen and Jones, 1998; Aravind et al., 2004; Leipe et al., 2004) giving these proteins their name: NB-LRR proteins.

The NB-ARC domain itself consists of three subdomains: a nucleotide-binding (NB) domain and a C-terminal extension that forms a four-helix bundle (ARC1) and a winged-helix fold (ARC2; Albrecht and Takken, 2006). Mutations in the NB-ARC domain often

[1] This work was supported by Bioseeds/Keygene (J.V.), the German Research Foundation (contract no. LE 491/14–1 to M.A. and T.L.), the German National Genome Research Network, and the BioSapiens Network of Excellence funded by the European Commission (grant no. LSHG–CT–2003–503265).

[2] These authors contributed equally to the paper.

[3] Present address: The Sainsbury Laboratory, John Innes Centre, Norwich Research Park, Colney, Norwich NR4 7UH, UK.

[4] Present address: Laboratory of Phytopathology, Wageningen University, Binnenhaven 5, 6709 PD Wageningen, The Netherlands.

* Corresponding author; e-mail takken@science.uva.nl; fax 31–20–5257934.

The author responsible for distribution of materials integral to the findings presented in this article in accordance with the policy described in the Instructions for Authors (www.plantphysiol.org) is: Frank L.W. Takken (takken@science.uva.nl).

Article, publication date, and citation information can be found at www.plantphysiol.org/cgi/doi/10.1104/pp.105.073510.

abolish R-protein function, signifying the functional relevance of this domain (Dinesh-Kumar et al., 2000; Tao et al., 2000; Tornero et al., 2002a). We have shown that the NB-ARC domains for tomato (*Lycopersicon esculentum*) R proteins I-2 and Mi-1 are functional ATPase modules that specifically bind and hydrolyze ATP in vitro (Tameling et al., 2002).

Besides R proteins, the NB-ARC domain is found in animal ATPases APAF-1 and CED-4, which are both involved in apoptosis, various bacterial transcription factors, and many uncharacterized proteins (Leipe et al., 2004). Together, these proteins represent a clade of the signal transduction ATPases with numerous domains (STAND) proteins (Leipe et al., 2004). The NB domain of these STAND proteins has the so-called P-loop NTPase fold. Two well-conserved motifs in the NB site of P-loop NTPases can be distinguished: the P-loop (also called the Walker A or kinase 1a motif) and the Walker B (kinase 2) motif (Walker et al., 1982; Saraste et al., 1990; Traut, 1994). The Walker A motif has the general consensus sequence $GX_4GK[T/S]$, wherein the invariant Lys residue is involved in coordination of the β- and γ-phosphates of the bound NTP. Mutation of this Lys of I-2 into an Arg (K207R) greatly reduced the ability of the protein to bind ATP (Tameling et al., 2002). The Walker B motif is less conserved; hhhhD and, in R proteins, hhhhDD (where h stands for hydrophobic residue). The first Asp in this motif is invariant and involved in coordination of the Mg^{2+} ion in the catalytic site. The second acidic residue, which is frequently present in this motif, is believed to act as the catalytic base for ATP hydrolysis (Muneyuki et al., 2000). Besides the Walker A and B motifs, the NB-ARC domain of R proteins contains three other conserved motifs with unknown function: resistance nucleotide-binding site (RNBS)-A, RNBS-D, and MHD (for Met, His, Asp; van der Biezen and Jones, 1998; Meyers et al., 1999, 2003; Pan et al., 2000a).

To further our understanding of the role of nucleotide binding and hydrolysis for R-protein function, we introduced mutations in the conserved motifs of the NB subdomain of the NB-ARC of I-2. The tomato R protein I-2 confers resistance to the fungal pathogen *Fusarium oxysporum* (Ori et al., 1997; Simons et al., 1998). Two mutations were identified that lead to HR in the absence of an elicitor (the elicitor for I-2 has not been identified yet). Biochemical analysis of the mutant proteins revealed that they were disturbed in their ATPase activity. Three-dimensional (3D) modeling of the ATPase domain showed that both mutations map near the predicted active site of the NB subdomain. To determine whether these mutants are affected in ATP binding or in ATP hydrolysis, their reaction kinetics were studied. These data indicate that, for R-protein activation, ATP binding, but not hydrolysis, is required. Although ATP hydrolysis appears not to be needed for induction of signaling, our data suggest that it plays an important role in keeping R-protein activity in check in the absence of plant pathogens. Furthermore, our experiments show that the NB-ARC domain adopts different conformations depending on the nucleotide bound (ATP or ADP), providing novel insight into the role this domain plays as a molecular switch for R-protein activation.

RESULTS

Point Mutations in the NB-ARC Domain of I-2 Result in Autoactivating Proteins

Little is known about the mode of action of the NB-ARC domain in plant R proteins. The NB-ARC domain of the tomato R protein I-2 contains five conserved motifs (i.e. the P-loop, the RNBS-A, the Walker B, the RNBS-D, and the MHD; van der Biezen and Jones, 1998; Meyers et al., 1999, 2003; Pan et al., 2000a; Fig. 1A). The first three motifs are present in the NB subdomain, whereas the latter two are located in the helical extension. Previously, we have shown that the NB-ARC domain comprises a functional ATPase module (Tameling et al., 2002). Here, we study the role of NB and hydrolysis activity of this domain for I-2 protein function; therefore, we introduced mutations at specific residues in the three conserved motifs (Table I) in the NB subdomain. These mutations were designed such that they could potentially negatively affect nucleotide binding and/or nucleotide hydrolysis. Two contiguous mutations were made in the P-loop; that is, the invariant Lys was substituted by Arg (K207R) and a highly conserved Thr was substituted by a Ser (T208S). In the RNBS-A motif, S233F was introduced because of the mutation S207F in the NB domain of the enhancer-binding protein NtrC from *Escherichia coli*. This S207F mutation in NtrC affected ATP hydrolysis, but did not affect nucleotide binding (Rombel et al., 1999). However, subsequent bioinformatics studies using sequence alignments revealed that this mutation in NtrC does not really correspond to S233F in I-2 as thought initially (data not shown). Furthermore, the Walker B motif was disrupted by mutating the two conserved Asp residues (i.e. D282C and D283E).

For I-2 and related R proteins (e.g. Rx and Mi-1), it has been shown previously that certain mutations can give autoactivation of the HR (a hallmark of plant disease resistance) upon expression in planta in the absence of the corresponding elicitor (Hwang et al., 2000; Bendahmane et al., 2002). In I-2, for example, the mutation D495V in the MHD motif gives an HR when transiently expressed in *Nicotiana benthamiana* (De la Fuente van Bentem et al., 2005; Table I; Fig. 1C), whereas expression of the wild-type I-2 protein does not trigger an HR (Fig. 1B). The ability of the D495V mutant to induce an HR is dependent on Hsp90, RAR1, and SGT1 (De la Fuente van Bentem et al., 2005). The *SGTI* dependence of the cell death phenotype is one of the characteristics of R-protein-mediated responses (Peart et al., 2002). Similarly, we transiently expressed each of the above-mentioned mutations (Table I) in *N. benthamiana* using agroinfiltration. The mutations K207R, T208S, and D282C did not give autoactivation of the defense

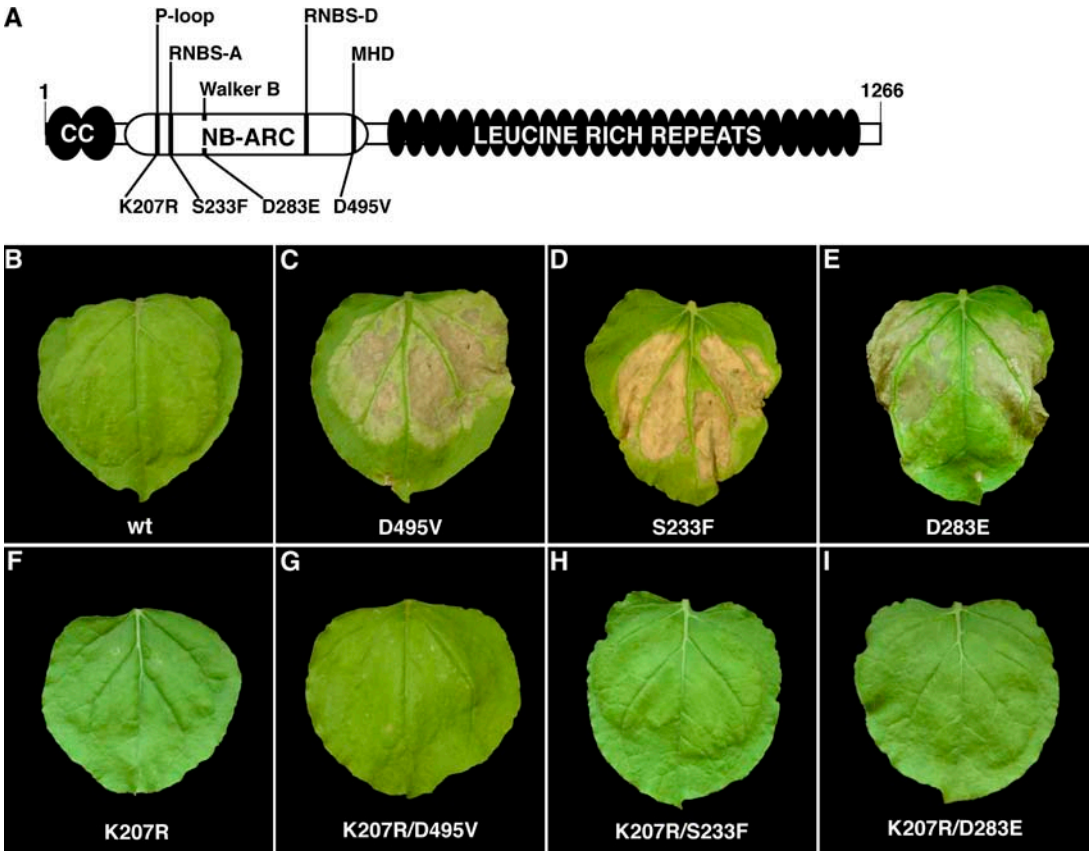

Figure 1. Selection of autoactivating mutations in I-2. A, Schematic representation of the tripartite modular structure of I-2, which consists of an N-terminal CC, a central NB-ARC, and a C-terminal LRR. In the indicated motifs, specific amino acids were subjected to mutational analysis to identify autoactivating proteins. Numbers indicate amino acid positions. B to I, Transient expression of wild type and a subset of mutant forms of *I-2* in *N. benthamiana* leaves via agroinfiltration. In B, the response to wild-type I-2 is depicted. Autoactivating mutants *I-2*^{D495V}, *I-2*^{S233F}, and *I-2*^{D283E} (C–E) induce a cell death response that is abolished when combined with the K207R mutation in the P-loop (F–I). Leaves were photographed 9 d after infiltration.

response resulting in macroscopically visible HR (Fig. 1F; data not shown), whereas both the S233F (RNBS-A motif) and D283E (Walker B motif) substitutions did (Fig. 1, D and E). Like D495V, the S233F mutant requires SGT1 to induce an HR (S. De la Fuente van Bentem, unpublished data). Compared to D495V, the onset of cell death was slower in S233F and D283E by 2 and 3 d, respectively.

Previously, we have shown that the invariant Lys (K207) in the P-loop of I-2 is essential for nucleotide binding (Tameling et al., 2002). The corresponding residue had also been shown to be required for resistance mediated by the R protein N of tobacco (*Nicotiana tabacum*) and the resistance to *Pseudomonas syringae* 2 (RPS2) and resistance to *Pseudomonas syringae* pv *maculicola* 1 (RPM1) R proteins of Arabidopsis (*Arabidopsis thaliana*; Dinesh-Kumar et al., 2000; Tao et al., 2000; Tornero et al., 2002a) and for autoactivation of Rx-MHV and L-MHV mutants (Bendahmane et al., 2002; Howles et al., 2005). To test whether an intact P-loop is required for HR triggered by the autoactivating mutations, double mutations were introduced in I-2 in which K207R was combined with either one of the three autoactivating substitutions. When transiently expressed in *N. benthamiana*, all three double mutants (K207R/D495V, K207R/S233F, and K207R/D283E), similar to the single K207R mutant, failed to induce an HR (Fig. 1, F–I). This result indicates that the ability of all three

Table I. *Motifs targeted for mutation and their effect in a transient expression assay*

Substitution	Motif	HR[a]
K207R	P-loop	−
T208S	P-loop	−
S233F	RNBS-A	+
D282C	Walker B	−
D283E	Walker B	+
D495V[b]	MHD	+

[a]HR, Hypersensitive response in *N. benthamiana* leaves upon agroinfiltration. HR was scored 9 d after infiltration. [b]Positive control for HR induction, mutation is described before (De la Fuente van Bentem et al., 2005).

autoactivating mutants to trigger HR depends on a functional P-loop able to bind nucleotides.

Two Autoactivating Mutants Display Reduced ATP Hydrolysis

Both autoactivating mutations, D283E and S233F, in the NB subdomain were subsequently subjected to a biochemical study to explore the role of nucleotide binding and ATP hydrolysis for I-2 function in activating an HR. Since full-length I-2 is unstable in *E. coli* and yields are extremely low, truncated forms of I-2 (I-2N, I-2N^{S233F}, and I-2N^{D283E}) were produced in *E. coli* that encompass the amino-terminal part of the protein (i.e. the CC and NB-ARC domains, but not the LRR domain; Tameling et al., 2002). Equal purity and similar yields were obtained for wild-type and mutant proteins (data not shown). We then quantified the intrinsic ATP-binding and ATPase activity of wild-type (average of two independently purified batches) and mutant proteins. For measuring ATPase activity, purified proteins were incubated at 25°C with varying concentrations of [α^{32}P]ATP. To measure the conversion of [α^{32}P]ATP into [α^{32}P]ADP in time, samples were taken at different time points and [α^{32}P]ATP and [α^{32}P]ADP were resolved by thin-layer chromatography (TLC). The conversion rate at each of the [α^{32}P]ATP concentrations was used to calculate the maximal initial hydrolysis rate (V_{max}) using standard Lineweaver-Burk plots. The V_{max} of wild-type I-2N was determined to be 6.2 ± 1.5 pmol ATP hydrolyzed min^{-1} μg^{-1} protein (Fig. 2A). The V_{max} values of I-2N^{S233F} and I-2N^{D283E} (Fig. 2A) were found to be 4.5- and 5-fold lower (1.4 ± 0.4 and 1.2 ± 0.2 pmol min^{-1} μg^{-1}), respectively, indicating that the mutants are impaired in their ATPase activity.

Reduced ATPase activity could be caused by a lower rate of ATP hydrolysis, including dissociation of product ADP, or by diminished ATP binding. Therefore, the K_m of the mutant and wild-type proteins was measured. Using the same Lineweaver-Burk plots, the K_m value (which represents the ATP concentration at half-maximal hydrolysis rate) was calculated for each protein. For wild-type I-2N, a K_m of 2.0 ± 0.2 μM was found (Fig. 2B). For I-2N^{S233F} and I-2N^{D283E}, slightly lower values of 1.3 ± 0.2 μM and 1.8 ± 0.1 μM were measured, respectively (Fig. 2B). Such a small decrease of the K_m value fits very well with a lowered rate of the ATP hydrolysis reaction, but not with a lowered rate of ATP binding because $K_m = (k\text{-}1 + k_{cat})/k1$, where *k1* and *k-1* represent the rate constants for binding and dissociation of ATP, respectively. Thus, the lowered ATPase activity of the autoactivating mutants is not due to a lowered affinity of the enzyme for ATP, but to a diminished rate of ATP hydrolysis.

The S233F Mutation Results in a Compromised k_{cat}

The ATPase cycle consists of the following steps: (1) ATP binding, (2) ATP hydrolysis, and (3) dissociation of ADP from the active site:

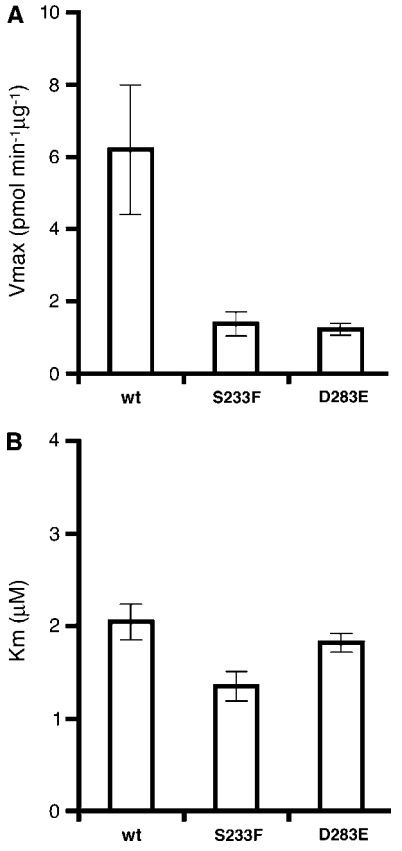

Figure 2. Hydrolysis rate (V_{max}) and affinity (K_m) of I-2N and its mutants for ATP. Purified I-2N and mutant forms of this protein (S233F and D283E) were incubated with different concentrations of [α^{32}P]ATP. Conversion of ATP to ADP was measured in an ATPase assay and quantified. The conversion rates at each ATP concentration were plotted in a Lineweaver-Burk graph and used to determine the V_{max} (pmol min^{-1} μg^{-1}; A) and K_m (μM; B). All reactions were done at least in duplicate. The V_{max} and K_m value of I-2N presented is the mean based on the outcome with two independently purified protein preparations; error bars indicate the SD.

$$\text{I-2N} + \text{ATP} \underset{K_m}{\longleftrightarrow} (\text{step 1})\ \text{I-2N}\cdot\text{ATP}$$

$$\text{I-2N}\cdot\text{ATP} \underset{k_{cat}}{\rightarrow} (\text{step 2})\ \text{I-2N}\cdot\text{ADP} + P_i$$

$$\text{I-2N}\cdot\text{ATP} \underset{k_{off-ADP}}{\longleftrightarrow} (\text{step 3})\ \text{I-2N} + \text{ADP}$$

As mentioned previously, both wild-type and autoactivating I-2 mutants display similar affinities (K_m) for ATP (step 1 in the cycle). However, unlike the wild type, these mutants were impaired in ATPase activity (shown by the lower V_{max}). This reduction could be caused by (1) a decreased hydrolysis rate (k_{cat}; step 2) or (2) an increased affinity of the mutants for ADP after hydrolysis (lower $k_{off\text{-}ADP}$; step 3). In the presence of ATP, a decreased hydrolysis rate will result in an accumulation of the I-2N·ATP complex, whereas an increased affinity for ADP (reduced $k_{off\text{-}ADP}$) will result in an accumulation of the I-2N·ADP complex. To test which explanation is correct, we determined the re-

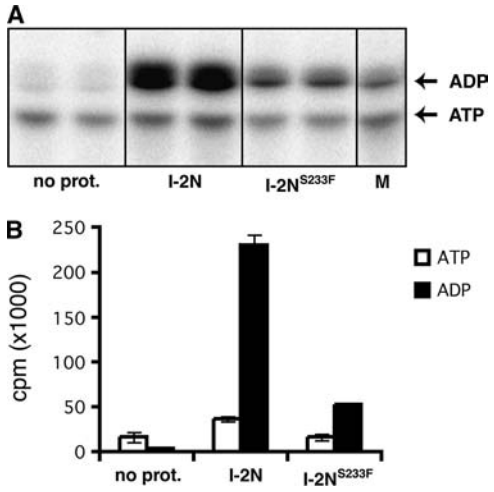

Figure 3. TLC of nucleotides bound to I-2N. [α^{32}P]ATP was incubated in duplicate either without protein (no prot.), with I-2N, or with the *I-2N^{S233F}* mutant. The nucleotides retained by I-2N on the filters were extracted and separated by TLC. Radioactivity of [α^{32}P]ATP and [α^{32}P]ADP was visualized by phosphor imaging (A) and quantified (B). The prevalent nucleotide bound by I-2N or I-2N^{S233F} is ADP. M, Marker of [α^{32}P]-labeled ATP and ADP.

lative amounts of ATP and ADP that are bound to I-2N. Therefore, we incubated on ice wild-type I-2N and I-2N^{S233F} with 2 μM [α^{32}P]ATP for 15 min. The samples were then spotted on polyvinylidene difluoride (PVDF) membranes and, after extensive washing, the nucleotides bound to the I-2N proteins were extracted under denaturing conditions. The extracted nucleotides were separated on TLC plates (Fig. 3A) and the amounts of [α^{32}P]ATP and [α^{32}P]ADP were quantified (Fig. 3B). For I-2N^{S233F}, the amount of bound ADP was reduced by approximately 70% compared to wild-type I-2N ($n = 9$, using two independent wild-type protein isolations). This reduction in the amount of bound ADP suggests that the reduced ATPase activity in the I-2N^{S233F} mutant is due to a lower hydrolysis rate (k_{cat}) rather than to an increased affinity for ADP (reduced $k_{off\text{-}ADP}$). Moreover, because the wild-type and mutant protein have similar ATP-binding affinities, this result implies that, under steady-state conditions, the mutant is likely to accumulate a relatively higher level of the I-2N·ATP state.

However, to our surprise, our analysis revealed only small amounts of ATP bound to both I-2N and I-2N^{S233F} (Fig. 3, A and B). Because similar (trace) amounts of ATP were found in the no-protein controls, the detected amounts of ATP are most likely due to nonspecific binding of ATP to the membrane rather than specific binding to the protein. This means that, under our experimental conditions in which the I-2N·ADP complex can readily be visualized, we are unable to detect the I-2N·ATP complex. This could be explained in two ways: (1) The bound ATP is hydrolyzed during the extraction procedure; or (2) in contrast to the I-2N·ADP complex, the I-2N·ATP complex is unstable, preventing its retention on the filter. To distinguish between these two options, we used a nonhydrolyzable ATP analog (ATP-γ-S), allowing us to measure solely the I-2N·ATP complex. Because this nucleotide analog has a slightly different structure, we first analyzed the affinity of I-2N for ATP-γ-S. Wild-type I-2N was added to mixtures of [α^{32}P]ATP with increasing amounts of either ATP or its nonhydrolyzable analog ATP-γ-S and these samples were subsequently analyzed in a filter-binding assay. Both nucleotides were able to compete for [α^{32}P]ATP binding with similar efficiencies (Fig. 4A), indicating identical affinities for both nucleotides and that ATP-γ-[^{35}S] can be used as a genuine I-2N substrate. However, after incubating I-2N with ATP-γ-[^{35}S] and subsequent washing in the filter-binding assay, we were unable to detect the I-2N·ATP-γ-[^{35}S] complex on the filters using liquid scintillation counting (data not shown). Also, nucleotide extraction from these filters revealed only background levels of radioactivity. These results support the second explanation that, in contrast to the I-2N·ADP complex, the I-2N·ATP complex is unstable and does not survive the washing procedure.

The relative ease at which the stable I-2N·ADP complex can be detected, as opposed to the I-2N·ATP complex, suggests a higher affinity of the wild-type I-2N protein for ADP than for ATP. However, when premixed with [α^{32}P]ATP, both ATP and ADP are able to compete for binding of [α^{32}P]ATP to I-2N with similar efficiency (Tameling et al., 2002), showing that ATP and ADP have similar initial binding affinities for the empty I-2N. The observed 70% reduction in the amount of ADP bound to the S233F mutant (Fig. 3B), together with the reduction in the k_{cat}, suggests that in the mutant the ADP/ATP equilibrium has relatively shifted to the ATP-bound state.

I-2N Bound to ADP Has a Different Conformation Than I-2N Bound to ATP

The instability of the I-2N·ATP complex (and the I-2N·ATP-γ-S complex) versus the stability of the measured I-2N·ADP complex suggests a conformational change of the protein resulting in an increased binding affinity for ADP. To investigate the I-2N·ADP complex further, its stability was measured. To this end, a filter-binding experiment was performed in which I-2N was incubated on ice with [α^{32}P]ATP. After 15 min, an excess of cold ATP was added and the mixture was further incubated for different periods of time. The relative amount of radioactivity retained on the filter ([α^{32}P]ADP) was plotted against the incubation time (Fig. 4B). Using this plot, the time at which 50% of the radioactivity had dissociated from the I-2N·ADP complex was calculated to be approximately 30 min ($t_{1/2}$ = 30 min). This extraordinarily long $t_{1/2}$ corresponds to a dissociation rate constant (k_{off}) of 3.9×10^{-4} s^{-1} ($k_{off} = \ln 2/t_{1/2}$) for I-2N·ADP. Such a low dissociation rate constant for the I-2N·ADP complex is not compatible

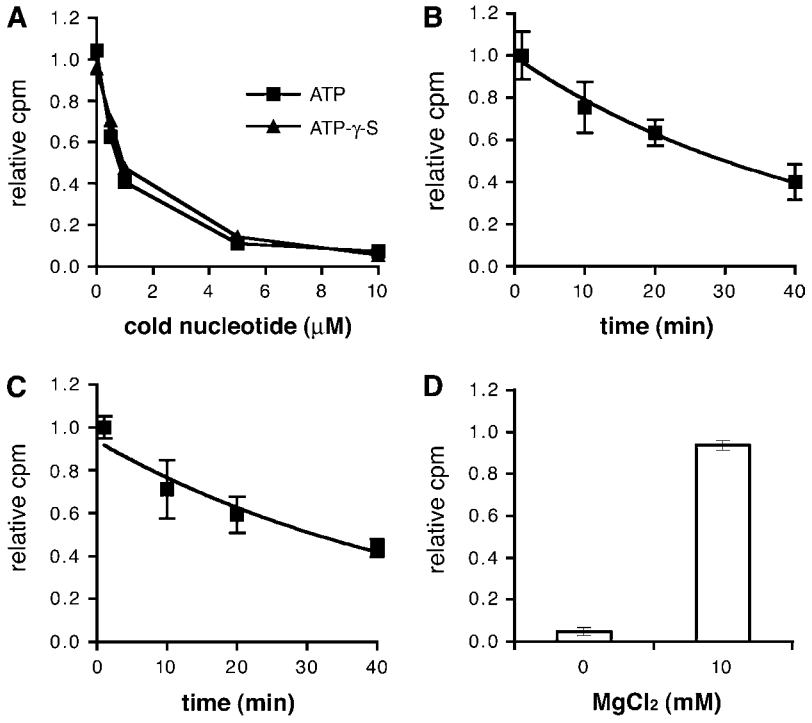

Figure 4. Stability of the I-2N·ADP complex. In filter-binding assays, radioactivity bound to wild-type I-2N was quantified and expressed as relative cpm. A, In a competition experiment, [α^{32}P]ATP was premixed with an increasing amount of either cold ATP or ATP-γ-S. This graph shows that both nucleotides compete equally well for binding. B, Determination of k_{off}. I-2N was incubated with [α^{32}P]ATP (for 15 min) and, after addition of an excess of cold ATP, samples were taken at different time points. From this graph, the half life of the I-2·ADP complex was estimated to be approximately 30 min. C, The same competition experiment as in B, but using [α^{32}P]ADP and an excess of cold ADP. This graph shows that ATP hydrolysis is not required to obtain a stable I-2N·ADP complex. D, The formation of the stable I-2N·ADP complex depends on Mg^{2+}. I-2N was incubated with [α^{32}P]ADP in the presence or absence of $MgCl_2$, and radioactivity bound to the protein was quantified.

with the previously measured affinity for ATP (K_d = 2 μM) for the empty I-2N protein (Tameling et al., 2002) because it would imply an association rate constant (k_{on}; $k_{on} = k_{off}/K_d$) of $1.91 \times 10^2\ M^{-1}\ s^{-1}$. Such a low k_{on} value is not in agreement with the observed binding kinetics of ATP or ADP to I-2N and the experimental findings can only be explained when the protein has two distinct conformations having different affinities and k_{off} values for ADP: an empty and ATP/ADP-bound state having a K_d of 2 μM with a relatively high k_{off} and a stable I-2N·ADP state with a much lower K_d and a very low k_{off} ($3.9 \times 10^{-4}\ s^{-1}$). Unfortunately, the K_d value of the latter complex cannot be measured directly because release of ADP causes the protein to return into its initial low-affinity state. Only indirect evidence for the existence of the stable complex, as determined by the low k_{off} value, can be obtained.

To answer the question of whether the formation of the stable I-2N·ADP complex requires ATP hydrolysis or whether direct ADP binding is also sufficient, filter-binding assays in which I-2N was incubated with either [α^{32}P]ADP or [α^{32}P]ATP were performed. In both cases, similar amounts of ADP were retained by I-2N, showing that ADP binding itself is sufficient for the formation of a stable I-2N·ADP complex and that ATP hydrolysis is not required (data not shown). To firmly establish that the complex formed by ADP binding is similar to the one that is formed by ATP hydrolysis, we repeated the filter-binding experiment as described above, but using [α^{32}P]ADP and cold ADP as competitor instead of [α^{32}P]ATP and cold ATP. From this experiment, the $t_{1/2}$ for ADP dissociation was calculated to be approximately 34 min (Fig. 4C). This value is similar to the 30 min found with [α^{32}P]ATP (Fig. 4B), confirming that ATP hydrolysis activity is not required for the formation of a stable I-2N·ADP complex per se, as direct ADP binding to the empty site also results in this stable complex.

Previously, we have shown that I-2, like other P-loop ATPases, requires Mg^{2+} as a cofactor for the hydrolysis of ATP (Tameling et al., 2002). To test whether Mg^{2+} is also required for the formation of the stable I-2N·ADP complex, a filter-binding assay with [α^{32}P]ADP was performed in the absence of Mg^{2+}. When Mg^{2+} was omitted from the reaction mixture, no radioactivity was retained on the filters (Fig. 4D), which indicates that Mg^{2+} is not only required for ATP hydrolysis (Tameling et al., 2002), but also for the formation of the stable I-2N·ADP complex. Based on these data, it is not possible to distinguish whether Mg^{2+} is required for initial binding of ADP or for the conformational change leading to the stable complex or both.

Autoactivating Mutations Cluster Together in a 3D Model of the NB Domain

To reveal the relative position of Ser-233 and Asp-283 in the 3D structure of I-2, closely related NB-ARC and NACHT domains of plant and human proteins were assembled into a structure-based multiple sequence alignment (Fig. 5A). The inclusion of both plant and human proteins allowed us to modify our previous alignment of human NACHT and NB-ARC domain proteins (Albrecht et al., 2003a). Based on structure prediction results from the BioInfo.PL metaserver and the associated 3D-Jury evaluation, including sec-

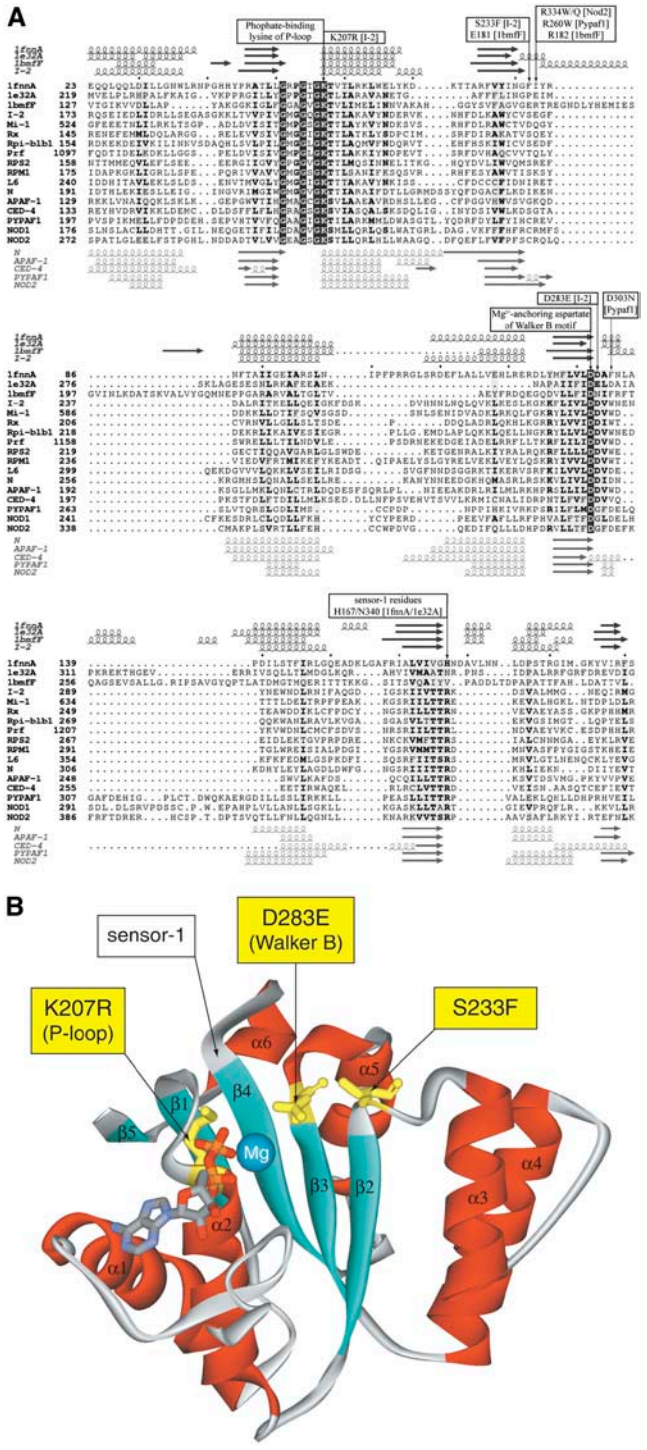

Figure 5. Structure-based multiple sequence alignment of the NB subdomain and structural model of this subdomain in I-2. A, Structure-based multiple sequence alignment of the NB subdomain of NB-ARC and NACHT domain proteins including the PDB structures 1fnnA, 1e32A, and 1bmfF. The DSSP secondary structure and the corresponding predictions by the PSIPRED server are depicted in the top and bottom part of each alignment row (α-helices are represented by curled lines, β-strands by horizontal arrows). Alignment columns with identical residues are highlighted in dark-gray boxes, those in which more than 60% of the residues are physicochemically conserved are shown in light-gray boxes. Mutations in I-2 and disease-associated mutations in Nod2 and Pypaf1 are denoted. Residues important in ATP binding and/or hydrolysis as well as the putative nucleotide sensor-1 residues (analogous to AAA+ proteins) are also annotated. B, Structural 3D model of the NB subdomain of I-2 (based on the template 1fnnA). α-Helices are colored in red and β-strands in blue; the locations of mutations are annotated in yellow and are shown as sticks together with the bound ADP and magnesium ion (Mg). α-Helices and β-strands are numbered according to the order in which they occur in the multiple sequence alignment.

ondary structure predictions, the x-ray crystal structure of the ATPase domain of the cell division control protein Cdc6 (Protein Data Bank [PDB] identifier 1fnnA; Liu et al., 2000) was chosen as the best modeling template for the NB domain of I-2 (Fig. 5A). This template structure was also used to model the ATPase domains of the NACHT domain proteins Nod2 and Pypaf1 (Albrecht et al., 2003a), which shows that NB-ARC and NACHT domains share very similar structures. Based on the alignment with Cdc6, a 3D model of the NB domain structure of I-2 bound to ADP could be constructed (Fig. 5B). In this model, Lys-207, Ser-233, and Asp-283 (marked yellow) cluster together in close proximity to the phosphates of ADP, suggesting that these residues could indeed be directly involved in ATP binding and/or hydrolysis. Our autoactivation mutations might indirectly affect hydrolysis by disrupting the binding pocket (S233F) or directly by preventing correct bonding to the catalytic water required for the nucleophilic attack, which is essential for hydrolysis of the β-γ phosphate bond (D283E). It might also directly interfere with nucleotide binding (K207R).

DISCUSSION

Downstream Signaling of I-2 Requires ATP Binding

Previously, we have shown that the NB-ARC domain of I-2 functions as an ATPase (Tameling et al., 2002) allowing the protein to go through an ATP hydrolysis cycle. In this cycle, the protein binds and hydrolyzes ATP and subsequently releases ADP, allowing it to return to its empty state. Here, we provided data that ATP binding and not necessarily ATP hydrolysis by the NB-ARC domain may be the crucial step for R-protein activation. Mutagenesis of conserved motifs that together form the ATP-binding fold of the NB-ARC domain resulted in the identification of two mutations that lead to autoactivation of the defense response as manifested by a macroscopic HR, similar to I-2^{D495V} reported earlier (De la Fuente van Bentem et al., 2005). Both mutants, S233F and D283E, were affected in ATP hydrolysis but not in ATP binding (I-2^{D495V} has not been subjected to biochemical analysis because the mutation lies outside the NB subdomain). When we combined mutations S233F and D283E with a mutation in the P-loop that strongly reduces ATP binding (K207R; Tameling et al., 2002), HR was not induced in

N. benthamiana. From this, we conclude that activation of I-2 requires nucleotide binding to the NB subdomain prior to activation of downstream signaling. Moreover, because the two autoactivating mutants are disturbed in ATP hydrolysis (and hence likely accumulate in the ATP-bound state), the active conformation of I-2 able to initiate an HR might be the ATP-bound state. Such a model, in which the NTP-bound state of a protein is the active state, is analogous to that for other NB-signaling proteins such as the distantly related G-proteins, in which the GTP-bound state is the active state (Sprang, 1997).

We favor a model for I-2 function in which the resting or off state of the NB-ARC domain is represented by the ADP-bound state. The ATPase activity of I-2 would reset the protein from the ATP or on state to its off state, trapping ADP in the binding pocket. This idea agrees with the high stability of the I-2N·ADP complex compared to the instability of the I-2N·ATP complex (Fig. 3). The high stability is probably caused by a conformational change upon nucleotide binding because the initial NB affinities are equal for ATP and ADP as measured in competition assays (see "Results;" Tameling et al., 2002). This finding is reminiscent of the apparently highly stable ADP-bound state of APAF-1 (Riedl et al., 2005). Because direct ADP binding to the empty protein could also induce this conformational change, resulting in a stable I-2·ADP complex, hydrolysis is not required per se. However, in the cell, this change will probably rely on hydrolysis of ATP because ATP is by far the most prevalent nucleotide in vivo. Our data suggest that ATP binding is sufficient to switch the I-2 protein into the active conformation that triggers defense signaling.

This reaction scheme differs from that for the structurally related NB-ARC protein APAF-1. Binding cytochrome *c* to the WD-40 repeat domain of APAF-1 results in hydrolysis of bound dATP and subsequent exchange of the produced dADP by dATP/ATP (Kim et al., 2005). Both dATP hydrolysis and nucleotide exchange are essential for formation of the activated state of APAF-1 that is able to form the apoptosome (Kim et al., 2005). Recently, the crystal structure of CED-4, the *Caenorhabditis elegans* homolog of APAF-1, has been solved (Yan et al., 2005). Like APAF-1, CED-4 requires ATP binding for function; however, it has been reported that CED-4 is unable to hydrolyze or exchange the nucleotide, suggesting that in this protein ATP binding could merely have a structural role (Yan et al., 2005). Pop and Salvesen (2005) suggested that these data could mean either that evidence for hydrolysis or nucleotide exchange has been missed for CED-4 or that indeed conformational cycling of this NB-ARC protein differs from that of APAF-1. In the latter case, this would imply that, although the NB-ARC domains of I-2, APAF-1, and CED-4 are structurally related, they seem to regulate the activity of the complete protein in different ways. However, the common theme in the regulation would be that their active state requires a NB pocket that is bound to ATP.

Autoactivating Mutations Inhibit ATPase Activity, Locking I-2 in the On State

To gain insight into how the autoactivating mutations may affect ATP hydrolysis, an alignment of the I-2 NB-ARC domain was assembled with related proteins of the NB-ARC and NACHT clade, both belonging to the STAND family. The NB-ARC domain consists of three subdomains: the two C-terminal subdomains called ARC1 and ARC2 (Albrecht and Takken, 2006) and the N-terminal ATPase domain that forms a 3D structure consisting of a parallel β-sheet flanked by α-helices (Albrecht et al., 2003a; Fig. 5B). The proposed model is very similar to the crystal structure of APAF-1 bound to ADP (Riedl et al., 2005). The ATPase fold of I-2 corresponds to the core structure of P-loop-containing NTPases (Vetter and Wittinghofer, 1999). Our 3D model of the ATPase domain of I-2 predicts that the mutations leading to constitutive activity, S233F and D283E, cluster together at the surface near the bound nucleotide (Fig. 5B).

S233F substitutes a Ser that is part of a conserved region referred to as the RNBS-A motif (Meyers et al., 1999; Pan et al., 2000b) and maps close to mutations associated with autoinflammatory disease in the NACHT domains of Nod2 (R334W/Q) and Pypaf1 (R260W). These latter mutations have been shown to cause constitutive activation as well (Chamaillard et al., 2003; Dowds et al., 2004; Tanabe et al., 2004). Similar mutations in the β-subunit of the F_1-ATPase (E181 and R182, PDB structure 1bmf, chain F) were also shown to affect ATP hydrolysis (Senior et al., 2002). Together, these findings indicate that the S233F mutation disturbs an essential and conserved region required for ATP hydrolysis in R and possibly in other STAND proteins. The D283E mutation in I-2 targets the second Asp of the Walker B motif that, in R proteins, as well as in AAA+ proteins like Cdc6 (1fnnA; Liu et al., 2000), ATP-binding cassette (ABC) transporters, and helicases, has the consensus hhhhD-D/E (where h is mostly a hydrophobic residue). The second acidic residue is believed to act as the general catalytic base in ATP hydrolysis (Muneyuki et al., 2000). In several ATPases (e.g. Cdc6, helicases, and ABC transporters), this residue was indeed found to be important for hydrolysis (Herbig et al., 1999; Orelle et al., 2003; for review, see Geourjon et al., 2001). The strict conservation of this Asp residue in the NB subdomain of NB-LRR proteins suggests that this residue may also act as the catalytic base in ATP hydrolysis in NB-LRR proteins.

The biochemical basis for the autoactivation of the D495V mutation is not known. The mutation lies close to the C terminus of the ARC2 subdomain and is part of the conserved MHD motif. In the structurally related APAF-1 protein, the imidazol residue from the analogous His forms a hydrogen bond with the β-phosphate of the bound ADP (Riedl et al., 2005). Riedl and coworkers (2005) propose that this residue not only coordinates the nucleotide, but also connects the ARC2 subdomain to the binding pocket, thereby

deeply burying ADP. Because of the significant, but weak, interaction of ARC2 with ADP, they suggest that this domain is prone to conformational changes. It is tempting to speculate that the MHD motif in I-2 has a similar function. The autoactivation phenotype caused by the D495V substitution would then be due to destabilization of ADP binding. This would allow the I-2 protein to release ADP, bind ATP, and hence switch to its active state in the absence of an elicitor. Currently, we are investigating this possibility.

Novel Intramolecular Interactions

Moffett and coworkers recently proposed a model for R-protein activation based on intramolecular interactions in the R-protein Rx, also a CC-NB-LRR (Moffett et al., 2002). They were able to demonstrate that the NB-ARC domain of Rx interacts with the LRR domain and likely with the CC domain as well (CC interacts with the NB-LRR part). The interaction with the LRR is disrupted upon recognition of the virally encoded avirulence protein that serves as the elicitor of the Rx-mediated defense response. So far, our attempts to perform similar experiments were unsuccessful because we have not been able to detect full-length I-2 or truncated versions of I-2 produced in planta using polyclonal antibodies raised against part of the ARC2 subdomain. Also N- or C-terminal versions of epitope-tagged I-2 expressed in planta could not be detected upon immunoprecipitations or pull-down assays. Nevertheless, we believe that the role of the NB-ARC domain in I-2 is consistent with the observations made for Rx.

We here propose a refined model for R-protein function in which the NB-ARC plays a pivotal role in regulating signaling (Fig. 6). As proposed for Rx, the resting state of the R protein is represented by a situation where the NB-ARC domain interacts with both the CC and LRR domain. This interaction requires a functional P-loop as observed for Rx. Moreover, we could show that I-2 function also requires an intact P-loop (K207R mutant). The switch from the off (ADP) to the on (ATP) state is triggered by either direct or indirect recognition of the elicitor. For Rx, this results in dissociation of the LRR from the CC-NB-ARC part of the protein. Our data would add that elicitor perception by the LRR domain triggers a conformation change in the NB-ARC domain leading to destabilization of the ADP-bound state (step 1), allowing rapid dissociation of ADP (step 2). A positive regulatory function of the LRR domain can be deduced from the observation that deletion of the LRR does not result in constitutive activity for Rx (Moffett et al., 2002), the I-2 wild type, or the hydrolysis mutants (data not shown). Also, many truncated and splice variants of R proteins that lack an LRR are encoded by the plant genome and these variants do not spontaneously induce a defense response (Lawrence et al., 1995; Anderson et al., 1997; Parker et al., 1997; Ayliffe et al., 1999; Dinesh-Kumar et al., 2000). A positive regulatory function for the LRR also fits with the finding that the elicitor-independent HR, triggered by a constitutively active Mi-1 chimera, could be abolished by numerous independent mutations in this domain (Hwang and Williamson, 2003). Furthermore, a positive regulatory function for the LRR can be inferred from our observation that in vitro the I-2N form, lacking the LRR domain, has a low, instead of a high, dissociation rate for ADP.

The next step in the ATPase cycle is binding of ATP (step 3). Our data indicate that the conformation of the ADP-bound state is different from that of the ATP-bound state. In the case of Rx, activation by the elicitor leads to dissociation of the CC domain from the NB-ARC domain (Moffett et al., 2002). This might be the key event for activation of downstream defense-

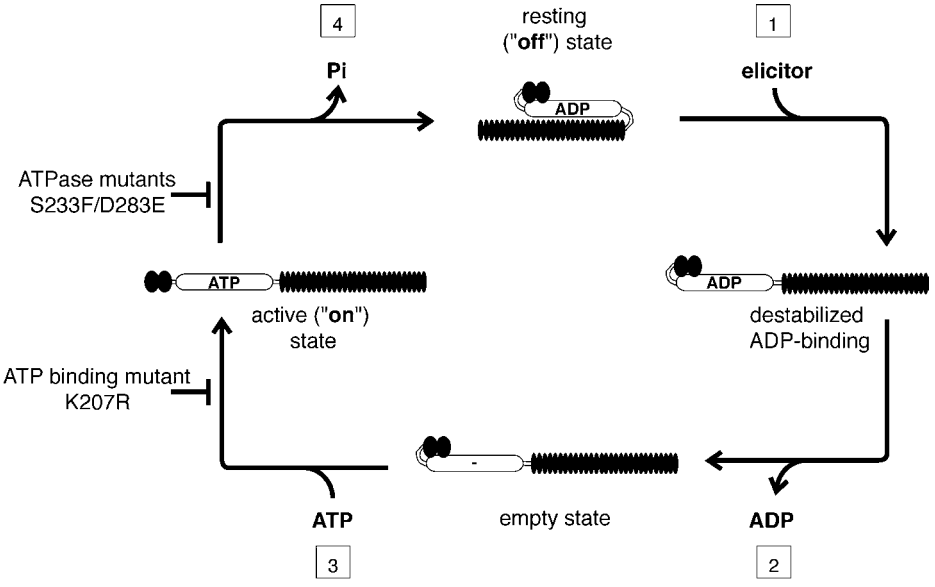

Figure 6. Proposed model of the NB-ARC domain functioning as a molecular switch in the regulation of R-protein-mediated signaling. In the resting (off) state, the CC and LRR domains are bound to the NB-ARC domain. The NB-ARC tightly binds ADP and this interaction is stabilized by the LRR domain. (1) Upon elicitor recognition, the LRR-NB-ARC interaction is disturbed, resulting in reduced affinity for ADP. (2) This reduced affinity results in rapid dissociation of ADP. (3) The free state binds ATP that triggers a conformational change, resulting in disruption of the CC-NB-ARC interaction. This active (on) state is competent to activate signaling, leading to induction of defense responses. (4) Hydrolysis of the bound ATP by the intrinsic ATPase activity returns the protein to its resting state. The steps affected by the mutations in the NB subdomain are indicated.

signaling pathways by allowing the R protein to interact with downstream-signaling partners (Belkhadir et al., 2004).

Hydrolysis of the bound ATP by the intrinsic ATPase activity (step 4) brings the protein back into its resting (off) state completing the ATPase cycle. We propose that this ATPase cycle also runs in vivo, albeit at a lower speed, in the absence of the pathogen. Evidence for that is the observation that there is a certain degree of constitutive activity of *R*-gene pathways in plants in the absence of elicitors (for review, see Nimchuk et al., 2003), resulting in an overall fitness penalty (Korves, 2004). A change in the reaction speed of any of the different steps in the ATPase cycle, either by pathogen perception or mutations in the NB-ARC domain, will influence the amount of I-2·ATP. Presumably, when the concentration of this complex exceeds a certain threshold, defense signaling will be initiated. This dynamic behavior of R proteins can explain why small disturbances in the amount of R protein in the cell can result in induction of defense signaling (Jin et al., 2002; Tornero et al., 2002b; Bieri et al., 2004). The fact that no HR is observed upon transient expression of wild-type I-2 in *N. benthamiana* indicates that, in this case, this threshold is not exceeded. It agrees with the finding that very low amounts of I-2 protein are produced in planta because the levels are below our detection levels. In summary, it is likely to be of crucial importance to the plant to tightly regulate the expression levels of R proteins.

Downstream Signaling

How the proposed active, ATP-bound state of I-2 triggers downstream signaling is not known. The related AAA+ ATPase proteins often rely on oligomerization for function (for review, see Hanson and Whiteheart, 2005) and oligomerization has also been shown for several STAND proteins, including MalT, APAF-1, C2TA, and Nod1 (for review, see Leipe et al., 2004). Recently, for the tobacco N R protein, a TIR-NB-LRR protein, it was shown that oligomerization is induced in the presence of the elicitor (Mestre and Baulcombe, 2006). So far oligomerization has not been shown for CC-NB-LRR proteins, and an alternative mechanism could be that the activated, NTP-bound state of the protein functions as a monomer, similar to G-proteins (Sprang, 1997).

Future experiments may reveal the molecular mechanism through which activated R proteins trigger downstream signal transduction cascades. In addition, more direct measurements of changes in protein conformation are required to establish how the nucleotide state controls this conformation and thereby the activity of the protein. Furthermore, we need to understand the switch function of the NB-ARC domain in relation to intramolecular interactions and other factors that may influence the rate of hydrolysis and nucleotide exchange similar to what has been found for G-proteins (Sprang, 1997).

MATERIALS AND METHODS

Constructs

Mutations were introduced by overlap extension PCR (Higuchi et al., 1988) using I-2 as a template. For each mutation, two flanking primers and the following set of mismatch primers were used: T208S (5′-CCAGGGCAAGTCTACACTTGC and 5′-GCAAGTGTAGACTTGCCCTGG); S233F (5′-TGGTATTGCGTTTTTGAAGGATTTGA and 5′-TCAAATCCTTCAAAAACGCAATACCA); D282C (5′-TCCTTATTGTTTTGTGTGATGTGTGGA and 5′-TCCACACATCACACAAAACAATAAGGA); and D283E (5′-TCCTTATTGTTTTGGATGAAGTGTGGA and 5′-TCCACACTTCATCCAAAACAATAAGGA) All mutations were confirmed by sequence analysis. All fragments were digested with *Nco*I and *Tth*111I to replace the corresponding fragment in the yeast (*Saccharomyces cerevisiae*) two-hybrid bait vector pAS2-1 (CLONTECH Laboratories) containing I-2N (1–519; described in De la Fuente van Bentem et al., 2005; herein referred to as CC-NB-ARC). Restriction fragments containing the mutation were excised from these vectors with *Sal*I and *Bam*HI to replace the corresponding fragments in the pGreen 1K-derived binary vector encoding full-length I-2F (1–1,266; WP42). In this vector, the gene is under the control of the cauliflower mosaic virus 35S promoter and a nopaline synthase transcription terminator. WP42 and the binary vector harboring I-2F^{D495V} (WP45) are described in De la Fuente van Bentem et al. (2005). The *Sal*I-*Bam*HI fragments containing the sequences coding for the S233F and D283E mutations were used to replace the corresponding fragments in I-2 present in the *Escherichia coli* expression vector pGEX-KG (Tameling et al., 2002). In this article, construction of pGEX-KG containing the *I-2N*^{K207R} mutant is described. To construct the binary vector that contains *I-2F*$^{K207R/D495V}$, the *Sal*I-*Bam*HI fragment containing the K207R mutation was isolated from the pGEX-KG construct containing *I-2N*^{K207R}, and used to replace the corresponding fragment in WP45. The pGEX-KG construct was used as a template for overlap extension PCR, as described above, to gain DNA fragments containing a second mutation coding for either S233F or D283E. These fragments were digested with *Sal*I and *Bam*HI and used to replace the corresponding fragment in WP42. This resulted in pGreen 1K containing the double mutants *I-2F*$^{K207R/S233F}$ and *I-2F*$^{K207R/D283E}$.

Agroinfiltration

All binary vector (pGreen 1K derived) constructs were transformed to *Agrobacterium tumefaciens* GV3101 and agroinfiltration was performed as described in Van der Hoorn et al. (2000). The cells were spun down and resuspended to an OD_{600} of 2. *Nicotiana benthamiana* plants used for infiltration were 4 to 5 weeks old. Plants were grown in a greenhouse at 25°C under supplemental lighting.

Multiple Sequence Alignment and Structural Modeling

Protein sequences were retrieved from the UniProt (Apweiler et al., 2004) database and protein domain architectures from the Pfam (Bateman et al., 2004) and SCOP (Andreeva et al., 2004) databases. The synonymous names of the protein sequences and UniProt accession numbers are as follows: I-2, Q9XET3; Mi-1, O81137; Rx, Q9XGF5; Prf, Q96485; Rpi-blb1/RGA2, Q7XBQ9; RPM1, Q39214; RPS2, Q42484; N, Q40392; L6, Q40253; PYPAF1/CIAS1/CRYOPYRIN/NALP3, Q96P20; NOD1/CARD4, Q9Y23; NOD2/CARD15/IBD1, Q9HC29; PYPAF2/NALP2/NBS1/PAN1, Q9NX02; PYPAF3/NALP7/NOD12, Q8WX94; PYPAF4/NALP4/PAN2, Q96MN2; PYPAF5/NALP6/PAN3, P59044; PYPAF6/NALP11/NOD17, P59045; PYPAF7/MONARCH-1/NALP12/PAN6, P59046; PYPAF8/MATER/NALP5, P59047; DEFCAP/CARD7/NALP1/NAC, Q9C000; CLAN/CARD12/IPAF, Q9NPP4; and CIITA/MHC2TA, P33076.

Protein structures were obtained from the PDB database (Bourne et al., 2004). The secondary structure assignments of PDB structures were taken from the DSSP database (Kabsch and Sander, 1983). A single capital letter appended to the actual PDB identifier denotes the chosen structure chain. The state-of-the-art online server PSIPRED (McGuffin et al., 2000) predicted the secondary structure of NB-ARC and NACHT domain proteins. Because of recent improvements of the PSIPRED method, we also recomputed the secondary structure of NACHT domain proteins discussed in our previous studies (Albrecht et al., 2003a, 2003b). The structure-based multiple sequence alignment of NB-ARC and NACHT domain proteins (Fig. 5A) was assembled using precomputed Pfam domain alignments and T-COFFEE (Poirot et al., 2003). We also im-

proved them manually by minor adjustments based on structure prediction results and pairwise superpositions of all PDB structures. The respective superpositions were computed by the program CE (Shindyalov and Bourne, 1998). For the alignment construction, we used the sequences of the NB-ARC domain proteins I-2, Mi-1, Rx, Rpi-blb1, Prf, RPS2, RPM1, L6, N, APAF-1, and CED-4 and the NACHT domain proteins PYPAF1-8, DEFCAP, CLAN, CIITA, and NOD1/2. In addition, the more distantly related structure of the β-subunit of the F_1-ATPase (PDB identifier 1bmfF) was included because the role of its functionally relevant amino acids has been investigated in detail. Furthermore, we investigated the results of all state-of-the-art fold recognition methods available via the online metaserver BioInfo.PL (Bujnicki et al., 2001), which contacts a dozen other prediction servers (whose names are listed on the Web site http://Bioinfo.PL/Meta). The associated 3D-Jury system allows for the comparison and evaluation of the predicted 3D models in a consensus view (Ginalski and Rychlewski, 2003). To obtain a 3D model of the NB domain structure of I-2, we extracted the sequence structure alignment of I-2 to 1fnnA from the multiple sequence alignment of NB-ARC and NACHT domain proteins (Fig. 5A) and submitted it to the 3D modeling server WHAT IF (Rodriguez et al., 1998). An alternative modeling template with a very similar structure despite low sequence identity would have been the vasolin-containing protein VCP, also known as membrane fusion ATPase p97 (PDB identifier 1e32A; Zhang et al., 2000). Further possible templates would be the crystal structures of APAF-1 and CED-4, which were published after the completion of this study (Riedl et al., 2005; Yan et al., 2005). The sequence alignments depicted in the figures were prepared in the SEAVIEW editor (Galtier et al., 1996) and illustrated by the Web service ESPript (Gouet et al., 2003). The protein structure images were drawn in the Accelrys Discovery Studio ViewerLite.

Purification of Glutathione *S*-Transferase Fusion Proteins from *E. coli*

I-2N, I-2N^{K207R}, I-2N^{S233F}, and I-2N^{S283E} were expressed as glutathione *S*-transferase fusions from the pGEX-KG-derived constructs in *E. coli*. Expression, purification, and renaturation were performed as described previously (Tameling et al., 2002). Protein concentration was determined by the Bradford method using bovine serum albumin as a standard.

ATPase Assay

ATPase assays were performed as described previously (Tameling et al., 2002). To measure the V_{max} and K_m at 25°C, either 42 or 118 ng active I-2N, I-2N^{K207R}, I-2N^{S233F}, and I-2N^{D283E} were incubated with three different [α^{32}P]ATP concentrations (0.6, 2, and 8 μM with specific activities of 7.4×10^5, 2.2×10^5, and 5.6×10^4 cpm/pmol, respectively) in a reaction volume of 16 μL. Samples were taken 0, 10, 20, and 40 min after starting the reaction. The amount of [α^{32}P]ADP and [α^{32}P]ATP in each sample was quantified from a TLC plate by using phosphor imaging (Storm; Molecular Dynamics). Data points were plotted and the hydrolysis speed (ν in pmol min^{-1}) for each reaction was determined by linear curve fitting. The speed values were used for each protein preparation to create Lineweaver-Burk plots from which the V_{max} (pmol ATP hydrolyzed min^{-1} μg^{-1} active protein) and K_m (μM) values were extracted.

[α^{32}P]ADP Production Using Hexokinase

[α^{32}P]ADP was produced by 5-min incubation at 25°C of [α^{32}P]ATP with 2 units of hexokinase (Sigma-Aldrich) in a reaction volume of 120 μL that contained 20 mM Tris-HCl, pH 8.0, 100 mM NaCl, 5 mM $MgCl_2$, and 100 mM Glc. To remove the hexokinase, the reaction was loaded on a microcon YM-10 filter unit (Millipore), centrifuged for 30 min at 13,000 rpm in a microcentrifuge, and subsequently washed with 100 μL water. The flow through was collected and the preparation was heated for 2 min at 100°C. No hexokinase activity could be detected in this final preparation. Full conversion to [α^{32}P]ADP was confirmed by TLC and the concentration was quantified using liquid scintillation counting.

Filter-Binding Assays

Filter-binding assays were performed according to Tameling et al. (2002), except that the reaction mixtures contained 10 mM $MgCl_2$.

Nucleotide Extraction from Filters

I-2N (0.31 μg active protein in 60 μL) or buffer only were incubated with 2 μM [α^{32}P]ATP (5.8×10^4 cpm/pmol) on ice and subjected to a filter-binding assay. Glycerol was omitted from the washing buffer, which did not affect ATP-binding characteristics. Deoxynucleotides were extracted from the filters by soaking them for 1 h in 700 μL 60% methanol (method adapted from Palmer and Cox, 1994). After incubation, 550 μL of the extracts were transferred to clean Eppendorf tubes and the liquid was evaporated using dry, flowing air. Pellets were dissolved in 10 μL water, of which 6 μL were used for TLC similar to that described for the ATPase assay (Tameling et al., 2002). [α^{32}P]ATP and [α^{32}P]ADP separated on the TLC plate were visualized by autoradiography using x-ray films (Fuji Photo Film) and the amount of radioactivity was quantified by using phosphor imaging (Storm; Molecular Dynamics).

Competition Filter-Binding Experiment

I-2N (0.24 μg active protein) was incubated for 15 min on ice with 0.15 μM [α^{32}P]ATP (5.8×10^5 cpm/pmol) and varying amounts of either cold ATP or ATP-γ-S (Fermentas and Roche) in 55-μL standard filter-binding reactions. Fifty microliters of the reactions were spotted on PVDF (Millipore) membranes and radioactivity was measured by liquid scintillation counting.

Nucleotide Dissociation Experiments

I-2N (0.18 μg active protein) was incubated on ice with 2 μM [α^{32}P]ATP (6.8×10^4 – 1.1×10^5 cpm/pmol) in 35-μL reaction mixtures. After 15 min, 20-μL reaction buffer containing 2.5 mM cold ATP was added (to dilute free [α^{32}P]ATP). These mixtures were incubated for different time periods prior to spotting on the PVDF membranes. To measure ADP dissociation, the same experiment was performed except that 2 μM [α^{32}P]ADP (2.65×10^4 cpm/pmol) and cold ADP were used.

Because of the apparent high stability of the I-2N·ADP complex, it was possible to measure the absolute amount of [α^{32}P]ADP bound to I-2N. This was done in triplicate at the concentration required for half-maximal binding (2 μM). The amount at saturation was calculated to deduce the amount of active protein in the preparation.

$MgCl_2$ Dependency of ADP Binding

I-2N (0.29 μg active protein) was incubated on ice with 0.2 μM [α^{32}P]ADP (7.6×10^4 cpm/pmol) in 55 μL of either standard reaction mixtures or mixtures without $MgCl_2$ added and in the presence of 10 mM EDTA (to chelate $MgCl_2$ [0.1 mM] carried over from the [α^{32}P]ADP preparation).

ACKNOWLEDGMENTS

We thank Martijn Rep, Harrold van den Burg, and David Baulcombe for critical reading of the manuscript and the referees of this paper for their useful comments.

Received October 28, 2005; revised January 25, 2006; accepted January 26, 2006; published February 17, 2006.

LITERATURE CITED

Albrecht M, Domingues FS, Schreiber S, Lengauer T (2003a) Structural localization of disease-associated sequence variations in the NACHT and LRR domains of PYPAF1 and NOD2. FEBS Lett **554:** 520–528

Albrecht M, Lengauer T, Schreiber S (2003b) Disease-associated variants in PYPAF1 and NOD2 result in similar alterations of conserved sequence. Bioinformatics **19:** 2171–2175

Albrecht M, Takken FLW (2006) Update on the domain architectures of NLRs and R proteins. Biochem Biophys Res Commun **339:** 459–462

Anderson PA, Lawrence GJ, Morrish BC, Ayliffe MA, Finnegan EJ, Ellis JG (1997) Inactivation of the flax rust resistance gene *M* associated with loss of a repeated unit within the leucine-rich repeat coding region. Plant Cell **9:** 641–651

Andreeva A, Howorth D, Brenner SE, Hubbard TJ, Chothia C, Murzin AG (2004) SCOP database in 2004: refinements integrate structure and sequence family data. Nucleic Acids Res **32:** D226–D229

Apweiler R, Bairoch A, Wu CH, Barker WC, Boeckmann B, Ferro S, Gasteiger E, Huang H, Lopez R, Magrane M, et al (2004) UniProt: the universal protein knowledgebase. Nucleic Acids Res **32:** D115–D119

Aravind L, Iyer LM, Leipe DD, Koonin EV (2004) A novel family of P-loop NTPases with an unusual phyletic distribution and transmembrane segments inserted within the NTPase domain. Genome Biol **5:** R30

Ayliffe MA, Frost DV, Finnegan EJ, Lawrence GJ, Anderson PA, Ellis JG (1999) Analysis of alternative transcripts of the flax *L6* rust resistance gene. Plant J **17:** 287–292

Bateman A, Coin L, Durbin R, Finn RD, Hollich V, Griffiths-Jones S, Khanna A, Marshall M, Moxon S, Sonnhammer EL, et al (2004) The Pfam protein families database. Nucleic Acids Res **32:** D138–D141

Belkhadir Y, Subramaniam R, Dangl JL (2004) Plant disease resistance protein signaling: NBS-LRR proteins and their partners. Curr Opin Plant Biol **7:** 391–399

Bendahmane A, Farnham G, Moffett P, Baulcombe DC (2002) Constitutive gain-of-function mutants in a nucleotide binding site-leucine rich repeat protein encoded at the *Rx* locus of potato. Plant J **32:** 195–204

Bieri S, Mauch S, Shen QH, Peart J, Devoto A, Casais C, Ceron F, Schulze S, Steinbiss HH, Shirasu K, et al (2004) RAR1 positively controls steady state levels of barley MLA resistance proteins and enables sufficient MLA6 accumulation for effective resistance. Plant Cell **16:** 3480–3495

Bourne PE, Addess KJ, Bluhm WF, Chen L, Deshpande N, Feng Z, Fleri W, Green R, Merino-Ott JC, Townsend-Merino W, et al (2004) The distribution and query systems of the RCSB protein data bank. Nucleic Acids Res **32:** D223–D225

Bujnicki JM, Elofsson A, Fischer D, Rychlewski L (2001) Structure prediction meta server. Bioinformatics **17:** 750–751

Chamaillard M, Girardin SE, Viala J, Philpott DJ (2003) Nods, Nalps and Naip: intracellular regulators of bacterial-induced inflammation. Cell Microbiol **5:** 581–592

Dangl JL, Jones JDG (2001) Plant pathogens and integrated defence responses to infection. Nature **411:** 826–833

De la Fuente van Bentem S, Vossen JH, de Vries K, van Wees SC, Tameling WIL, Dekker H, de Koster CG, Haring MA, Takken FLW, Cornelissen BJC (2005) Heat shock protein 90 and its co-chaperone protein phosphatase 5 interact with distinct regions of the tomato I-2 disease resistance protein. Plant J **43:** 284–298

Dinesh-Kumar SP, Tham WH, Baker BJ (2000) Structure-function analysis of the tobacco mosaic virus resistance gene N. Proc Natl Acad Sci USA **97:** 14789–14794

Dowds TA, Masumoto J, Zhu L, Inohara N, Nunez G (2004) Cryopyrin-induced interleukin 1beta secretion in monocytic cells: enhanced activity of disease-associated mutants and requirement for ASC. J Biol Chem **279:** 21924–21928

Ellis J, Dodds P, Pryor T (2000) Structure, function and evolution of plant disease resistance genes. Curr Opin Plant Biol **3:** 278–284

Feys BJ, Parker JE (2000) Interplay of signaling pathways in plant disease resistance. Trends Genet **16:** 449–455

Galtier N, Gouy M, Gautier C (1996) SEAVIEW and PHYLO_WIN: two graphic tools for sequence alignment and molecular phylogeny. Comput Appl Biosci **12:** 543–548

Geourjon C, Orelle C, Steinfels E, Blanchet C, Deleage G, Di Pietro A, Jault JM (2001) A common mechanism for ATP hydrolysis in ABC transporter and helicase superfamilies. Trends Biochem Sci **26:** 539–544

Ginalski K, Rychlewski L (2003) Detection of reliable and unexpected protein fold predictions using 3D-Jury. Nucleic Acids Res **31:** 3291–3292

Gouet P, Robert X, Courcelle E (2003) ESPript/ENDscript: extracting and rendering sequence and 3D information from atomic structures of proteins. Nucleic Acids Res **31:** 3320–3323

Hanson PI, Whiteheart SW (2005) AAA+ proteins: have engine, will work. Nat Rev Mol Cell Biol **6:** 519–529

Herbig U, Marlar CA, Fanning E (1999) The Cdc6 nucleotide-binding site regulates its activity in DNA replication in human cells. Mol Biol Cell **10:** 2631–2645

Higuchi R, Krummel B, Saiki RK (1988) A general method of in vitro preparation and specific mutagenesis of DNA fragments: study of protein and DNA interactions. Nucleic Acids Res **16:** 7351–7367

Howles P, Lawrence G, Finnegan J, McFadden H, Ayliffe M, Dodds P, Ellis J (2005) Autoactive alleles of the flax L6 rust resistance gene induce non-race-specific rust resistance associated with the hypersensitive response. Mol Plant Microbe Interact **18:** 570–582

Hwang CF, Bhakta AV, Truesdell GM, Pudlo WM, Williamson VM (2000) Evidence for a role of the N terminus and leucine-rich repeat region of the Mi gene product in regulation of localized cell death. Plant Cell **12:** 1319–1329

Hwang CF, Williamson VM (2003) Leucine-rich repeat-mediated intramolecular interactions in nematode recognition and cell death signaling by the tomato resistance protein Mi. Plant J **34:** 585–593

Inohara N, Nunez G (2003) NODs: intracellular proteins involved in inflammation and apoptosis. Nature Rev Immunol **3:** 371–382

Jin H, Axtell MJ, Dahlbeck D, Ekwenna O, Zhang S, Staskawicz B, Baker B (2002) NPK1, an MEKK1-like mitogen-activated protein kinase kinase kinase, regulates innate immunity and development in plants. Dev Cell **3:** 291–297

Kabsch W, Sander C (1983) Dictionary of protein secondary structure: pattern recognition of hydrogen-bonded and geometrical features. Biopolymers **22:** 2577–2637

Kim H-E, Du F, Fang M, Wang X (2005) Formation of apoptosome is initiated by cytochrome *c*-induced dATP hydrolysis and subsequent nucleotide exchange on APAF-1. Proc Natl Acad Sci USA **102:** 17545–17550

Korves T (2004) A novel cost of R gene resistance in the presence of disease. Am Nat **163:** 489–504

Lawrence GJ, Finnegan EJ, Ayliffe MA, Ellis JG (1995) The *L6* gene for flax rust resistance is related to the Arabidopsis bacterial resistance gene *RPS2* and the tobacco viral resistance gene *N*. Plant Cell **7:** 1195–1206

Leipe DD, Koonin EV, Aravind L (2004) STAND, a class of P-loop NTPases including animal and plant regulators of programmed cell death: multiple, complex domain architectures, unusual phyletic patterns, and evolution by horizontal gene transfer. J Mol Biol **343:** 1–28

Liu J, Smith CL, DeRyckere D, DeAngelis K, Martin GS, Berger JM (2000) Structure and function of Cdc6/Cdc18: implications for origin recognition and checkpoint control. Mol Cell **6:** 637–648

Martin GB, Bogdanove AJ, Sessa G (2003) Understanding the functions of plant disease resistance proteins. Annu Rev Plant Biol **54:** 23–61

McGuffin LJ, Bryson K, Jones DT (2000) The PSIPRED protein structure prediction server. Bioinformatics **16:** 404–405

Mestre P, Baulcombe DC (2006) Elicitor-mediated oligomerization of the tobacco N disease resistance protein. Plant Cell **18:** 491–501

Meyers BC, Dickerman AW, Michelmore RW, Sivaramakrishnan S, Sobral BW, Young ND (1999) Plant disease resistance genes encode members of an ancient and diverse protein family within the nucleotide-binding superfamily. Plant J **20:** 317–332

Meyers BC, Kozik A, Griego A, Kuang H, Michelmore RW (2003) Genome-wide analysis of NBS-LRR-encoding genes in Arabidopsis. Plant Cell **15:** 809–834

Meyers BC, Morgante M, Michelmore RW (2002) TIR-X and TIR-NBS proteins: two new families related to disease resistance TIR-NBS-LRR proteins encoded in Arabidopsis and other plant genomes. Plant J **32:** 77–92

Moffett P, Farnham G, Peart J, Baulcombe DC (2002) Interaction between domains of a plant NBS-LRR protein in disease resistance-related cell death. EMBO J **21:** 4511–4519

Muneyuki E, Noji H, Amano T, Masaike T, Yoshida M (2000) F(0)F(1)-ATP synthase: general structural features of ATP-engine and a problem on free energy transduction. Biochim Biophys Acta **1458:** 467–481

Nimchuk Z, Eulgem T, Holt BF III, Dangl JL (2003) Recognition and response in the plant immune system. Annu Rev Genet **37:** 579–609

Orelle C, Dalmas O, Gros P, Di Pietro A, Jault JM (2003) The conserved glutamate residue adjacent to the Walker-B motif is the catalytic base for ATP hydrolysis in the ATP-binding cassette transporter BmrA. J Biol Chem **278:** 47002–47008

Ori N, Eshed Y, Paran I, Presting G, Aviv D, Tanksley S, Zamir D, Fluhr R (1997) The *I2C* family from the wilt disease resistance locus *I2* belongs to the nucleotide binding, leucine-rich repeat superfamily of plant resistance genes. Plant Cell **9:** 521–532

Palmer S, Cox S (1994) Comparison of extraction procedures for high-performance liquid chromatographic determination of cellular deoxynucleotides. J Chromatogr A **667:** 316–321

Pan Q, Liu YS, Budai Hadrian O, Sela M, Carmel Goren L, Zamir D, Fluhr R (2000a) Comparative genetics of nucleotide binding site-leucine rich repeat resistance gene homologues in the genomes of two dicotyledons: tomato and Arabidopsis. Genetics **155:** 309–322

Pan Q, Wendel J, Fluhr R (2000b) Divergent evolution of plant NBS-LRR resistance gene homologues in dicot and cereal genomes. J Mol Evol **50:** 203–213

Parker JE, Coleman MJ, Szabo V, Frost LN, Schmidt R, Van Der Biezen EA, Moores T, Dean C, Daniels MJ, Jones JDG (1997) The Arabidopsis downy mildew resistance gene *Rpp5* shares similarity to the Toll and interleukin-1 receptors with *N* and *L6*. Plant Cell **9:** 879–894

Peart JR, Lu R, Sadanandom A, Malcuit I, Moffett P, Brice DC, Schauser L, Jaggard DA, Xiao S, Coleman MJ, et al (2002) Ubiquitin ligase-associated protein SGT1 is required for host and nonhost disease resistance in plants. Proc Natl Acad Sci USA **99:** 10865–10869

Poirot O, O'Toole E, Notredame C (2003) Tcoffee@igs: a web server for computing, evaluating and combining multiple sequence alignments. Nucleic Acids Res **31:** 3503–3506

Pop C, Salvesen GC (2005) The nematode death machine in 3D. Cell **123:** 192–193

Riedl SJ, Li W, Chao Y, Schwarzenbacher R, Shi Y (2005) Structure of the apoptotic protease-activating factor 1 bound to ADP. Nature **434:** 926–933

Rodriguez R, Chinea G, Lopez N, Pons T, Vriend G (1998) Homology modeling, model and software evaluation: three related resources. Bioinformatics **14:** 523–528

Rombel I, Peters-Wendisch P, Mesecar A, Thorgeirsson T, Shin YK, Kustu S (1999) MgATP binding and hydrolysis determinants of NtrC, a bacterial enhancer-binding protein. J Bacteriol **181:** 4628–4638

Saraste M, Sibbald PR, Wittinghofer A (1990) The P-loop—a common motif in ATP- and GTP-binding proteins. Trends Biochem Sci **15:** 430–434

Senior AE, Nadanaciva S, Weber J (2002) The molecular mechanism of ATP synthesis by F1F0-ATP synthase. Biochim Biophys Acta **1553:** 188–211

Shindyalov IN, Bourne PE (1998) Protein structure alignment by incremental combinatorial extension (CE) of the optimal path. Protein Eng **11:** 739–747

Simons G, Groenendijk J, Wijbrandi J, Reijans M, Groenen J, Diergaarde P, Van der Lee T, Bleeker M, Onstenk J, De Both M, et al (1998) Dissection of the fusarium *I2* gene cluster in tomato reveals six homologs and one active gene copy. Plant Cell **10:** 1055–1068

Sprang SR (1997) G protein mechanisms: insights from structural analysis. Annu Rev Biochem **66:** 639–678

Tameling WIL, Elzinga SD, Darmin PS, Vossen JH, Takken FLW, Haring MA, Cornelissen BJC (2002) The tomato *R* gene products *I-2* and *Mi-1* are functional ATP binding proteins with ATPase activity. Plant Cell **14:** 2929–2939

Tanabe T, Chamaillard M, Ogura Y, Zhu L, Qiu S, Masumoto J, Ghosh P, Moran A, Predergast MM, Tromp G, et al (2004) Regulatory regions and critical residues of NOD2 involved in muramyl dipeptide recognition. EMBO J **23:** 1587–1597

Tao Y, Yuan F, Leister RT, Ausubel FM, Katagiri F (2000) Mutational analysis of the Arabidopsis nucleotide binding site-leucine-rich repeat resistance gene RPS2. Plant Cell **12:** 2541–2554

Tornero P, Chao RA, Luthin WN, Goff SA, Dangl JL (2002a) Large-scale structure-function analysis of the Arabidopsis RPM1 disease resistance protein. Plant Cell **14:** 435–450

Tornero P, Merritt P, Sadanandom A, Shirasu K, Innes RW, Dangl JL (2002b) RAR1 and NDR1 contribute quantitatively to disease resistance in Arabidopsis, and their relative contributions are dependent on the R gene assayed. Plant Cell **14:** 1005–1015

Traut TW (1994) The functions and consensus motifs of nine types of peptide segments that form different types of nucleotide-binding sites. Eur J Biochem **222:** 9–19

van der Biezen EA, Jones JDG (1998) The NB-ARC domain: a novel signalling motif shared by plant resistance gene products and regulators of cell death in animals. Curr Biol **8:** R226–R227

Van der Hoorn RAL, Laurent F, Roth R, De Wit PJGM (2000) Agro-infiltration is a versatile tool that facilitates comparative analyses of Avr9/Cf-9-induced and Avr4/Cf-4-induced necrosis. Mol Plant Microbe Interact **13:** 439–446

Vetter IR, Wittinghofer A (1999) Nucleoside triphosphate-binding proteins: different scaffolds to achieve phosphoryl transfer. Q Rev Biophys **32:** 1–56

Walker JE, Saraste M, Runswick MJ, Gay NJ (1982) Distantly related sequences in the alpha- and beta-subunits of ATP synthase, myosin, kinases and other ATP-requiring enzymes and a common nucleotide binding fold. EMBO J **1:** 945–951

Yan N, Chai J, Lee ES, Gu L, Liu Q, He J, Wu JW, Kokel D, Li H, Hao Q, et al (2005) Structure of the CED-4-CED-9 complex provides insights into programmed cell death in *Caenorhabditis elegans*. Nature **437:** 831–837

Zhang X, Shaw A, Bates PA, Newman RH, Gowen B, Orlova E, Gorman MA, Kondo H, Dokurno P, Lally J, et al (2000) Structure of the AAA ATPase p97. Mol Cell **6:** 1473–1484